THERMAL, STRUCTURE AND PHASES ANALYSIS OF THE ALUMINIUM ENAC-$AlMg_5Si_2Mn$ ALLOY

Tomasz Tański[1], Mariusz Król[1], Przemysław Snopiński[1], Marek Roszak[1,*], Stanislav Rusz[2], Peter Palček[3]

[1] Institute of Engineering Materials and Biomaterials, Silesian University of Technology, ul. Konarskiego 18a, 44-100 Gliwice, Poland
[2] VŠB-Technical University of Ostrava, 17 listopadu 15, 708 33 Ostrava, Czech Republic
[3] Department of Materials Engineering, Faculty of Mechanical Engineering, University of Žilina, Univerzitná 1, 010 26 Žilina, Slovak Republic

[*] corresponding author: e-mail: marek.roszak@polsl.pl

Resume

The microstructure that is attributable from the specific casting method dictates further mechanical and physical properties of the material. In order to understand how to control the microstructure of the casting, it is important to understand the changes in microstructure during crystallization. The work focused on thermal analysis, metallurgical characterization and laser treatment of an aluminium alloy. The research show that the thermal analysis carried out on Universal Metallurgical Simulator and Analyser (UMSA) Technology Platform is an efficient tool for collect and calculates thermal parameters. The paper contributes to better understanding non-equilibrium metallurgical characterization of aluminium alloys. The solidification of the aluminium dendritic network, iron containing intermetallic phases, the aluminium-silicon eutectic and magnesium containing intermetallic phases were characterized.

Article info

Article history:
Received 4 October 2014
Accepted 1 April 2015
Online 16 May 2015

Keywords:
Manufacturing and processing;
Aluminium alloy;
Microstructure;
Thermal analysis;
EDS;
Phase identification;
Intermetallics;
Microstructural analysis.

Available online: http://fstroj.uniza.sk/journal-mi/PDF/2015/7-2015.pdf

ISSN 1335-0803 (print version)
ISSN 1338-6174 (online version)

1. Introduction

Currently, there is a huge amount of construction materials, but the demands placed on them are growing. Therefore, all the time is conducted intensive researches to develop new and better materials and technology. Aluminium alloys are the second after steel most commonly used materials representing an important group mainly used in aerospace and automotive industry where in nowadays the main requirement CO_2 reduction, thus, is necessary to use a new lighter materials [1 - 3].

In U.S., Europe and China, which are the biggest producers of cars, the priority issue is to reduce the total weight of the finished product through the use of lighter, more durable materials, and thereby reduce emissions of carbon dioxide into atmosphere. China plans to 2020 reduce the amount of fuel combustion up to 5 litters per 100 km, in Europe plan is to reduce CO_2 emissions into the atmosphere to 95 g/km, in the United States by 2025 a reduction of CO_2 emissions to a level of 101 g/km. It is most evident in the new generation of cars and so, for example, company which has now 19 % participation in world market [4] that produce one of the most popular model sold in the world - Volkswagen Golf – which IV generation weighed 1163 kg and after 15 years the current model VII generation weighs only 1150 kg, however,

is much more equipped, both in the corner types of security systems as well as devices that increase comfort, which is ensured by the use of modern materials, including the increased use of hot-formed steel with 5 to 20 %, and innovative solutions [5 - 10].

Aluminium alloys that combine low density and high strength are increasingly used in applications where weight reduction of components is important and cost effective. Due to its properties aluminium alloys are an attractive material for the applications where the main requirement is a high strength to density ratio [6, 7]. This makes it possible to design reliable, lightweight construction. However, designers needs pare rising so the important issue is the application of alloys with improved properties. It is expected that the use of aluminium alloys will increase, despite competition from plastic materials and composites [8 - 10]. Consequently, is necessary to develop high-strength alloys with a better properties and higher corrosive resistance [11 - 14].

Castings that contain different cross-section thicknesses result in different cooling rates, which, in turn, affect as-cast structure. In order to effectively control microstructure development during the melting, solidification as well as further materials processing is necessary to understand all metallurgical phenomena taking place. Knowledge of the solidification process as well as the influence of liquid and/or semi-solid metal treatment on micro and macro structure characteristic is of primary importance [15 - 18].

Thermal derivation analysis is very broad scope in both research and industrial practice. The most common application concerns a field of quality management because it allows rapid assessment of concentrations of certain elements in alloys, evaluation of some mechanical and technological properties, which in turn determines the quality of alloys. Thermal analysis is possible to perform alloy just before casting into the mould to make any adjustments to the quality of molten metal, e.g. for subsequent heating or cooling. The particular advantage this method is not only the opportunity to evaluate alloy with the chemical composition, but also the opportunity to evaluate the same process of measuring many of the details of the kinetics of crystallization of primary or secondary. Obtain as much information on interest in such a short time (2 - 5 minutes) allows for an immediate decision to improve the quality or the motivates greater technical discipline process. This is so the best and easiest way to improve the quality of foundry and metallurgical deciding the degree of reliability of machines and equipment [15, 17 - 20].

Heating and cooling curves can be described as the "metallurgical DNA" of the melting and solidification processes. Major and minor thermal events called metallurgical reactions that are thermodynamically strong enough in terms of the latent heat evolution that manifest themselves on the heating and cooling curves as inflection points and slope changes etc. can be determined [21 - 25].

2. Experimental procedure

2.1 Material

The investigations have been carried out on casting aluminium alloy ENAC-AlMg$_5$Si$_2$Mn - (ENAC-51500). Thanks to its very good properties found an application to high pressure castings and controlled vacuum castings, from which are produced body and engine parts in automotive industry.

Table 1

Average chemical composition (wt. %) of the ENAC-51500 aluminium alloy.

Fe	Si	Cu	Zn	Ti	Mn	Mg
0.120	1.900	0.005	0.010	0.009	0.580	5.170

Another advantage of this alloy is possibility to perform the heat treatment, which allows obtaining better properties. The chemical composition that was determined by the manufacturer of the investigated material is given in Table 1.

2.2 Test sample

The experiments were performed using a pre-machined cylindrical test sample with a diameter of $\phi = 18\ mm$ and height of $l = 20\ mm$ taken from the ingot. Each sample had a predrilled hole to accommodate a supersensitive K type thermocouple (with extra low thermal time constants) positioned at the centre of the test sample to registration the thermal data and control the processing temperatures. Thermocouples used in presented investigation were calibrated by the producer and delivered with certificates. Experiment was done under non-equilibrium conditions.

2.3 Thermal analysis

The thermal analysis during melting and solidification cycles was carried out using the Universal Metallurgical Simulator and Analyzer (UMSA) [21]. The melting and solidification experiments for the aluminium alloy were carried out using Argon as protective gas. The data for Thermal Analysis (TA) was collected using a high-speed National Instruments data acquisition system linked to a personal computer. Each TA trial was repeated three times for each of the three samples. The procedure comprised of the following steps. First, the test sample was heated to 700 ± 2 °C at heating rate approximately 0.8 °C/s and isothermally kept at this temperature for a period of 90 sec. in order to stabilize the melt conditions. Next, the test sample was solidified at cooling rate of approximately 0.5 °C/s, that was equivalent to the solidification process under natural cooling conditions.

The TA signal in the form of heating and cooling curves was recorded during the melting and solidification cycles. The temperature vs. time and first derivative vs. temperature were calculated and plotted. The cooling rates (CR) for these experiments were determined using the following formula (1):

$$CR = \frac{(T_{liq} - T_{sol})}{(t_{sol} - t_{liq})}\ (°C/s) \tag{1}$$

where T_{liq} and T_{sol} are the liquidus and solidus temperatures (°C), respectively, and t_{liq} and t_{sol} the times from the cooling curve that correspond to liquidus and solidus temperatures, respectively [22].

Accurate information concerning phase transformations are necessary to perform computer simulations of casting feedability and characterizations of the solidification process, as well as to make predictions concerning casting structure.

The α-Al Dendrite Nucleation Temperature ($T^{\alpha DEN}{}_{NUC}$), α-Al Dendrite Minimum (Undercooling) Temperature ($T^{\alpha DEN}{}_{MIN}$), α-Al Dendrite Coherency Point ($T^{\alpha DEN}{}_{DCP}$), α-Al Dendrite Growth Temperature ($T^{\alpha DEN}{}_{G}$), Al-Mg$_2$Si Eutectic Nucleation Temperature ($T^{AlSi}{}_{E,NUC}$), Al-Mg$_2$Si Eutectic Minimum Temperature ($T^{AlSi}{}_{E,MIN}$), Al-Mg$_2$Si Eutectic Growth Temperature ($T^{AlSi}{}_{E,G}$) and solidus temperatures T_{sol}, where calculated using the first derivative of the cooling curve [21 - 25]. Based on characteristics points from the thermal analysis, heat of phase transition individual phases was calculated. Heat capacity (c_p) of the alloy was determined using the following formula [25] (2):

$$c_p\,(t) = c_{p\,sol} \cdot \int_{t_N}^{t} (f_s(t)dt + c_{(p\,liq)}) \cdot \cdot (1 - \int_{t_N}^{t} (f_s(t)dt) \tag{2}$$

where: f_s – participation of fraction solid, t_n - time recorded where nucleation temperature occurs, considering that for $f_s\,(t \le t_N) = 0$ and $f_s\,(t \ge t_N) = 1$, $c_{p\ sol}$ – average heat capacity in solid state, $c_{p\ liq}$ – average heat capacity in liquid state.

Thermal-Calc Software (delivered by platform supplier) connected with UMSA platform was used to determine a specific heat capacity in liquid and solid state. Total heat of crystallization (Q) process of analysed alloys was calculated based on (3):

$$Q = c_p \cdot m \cdot \int_{t_N}^{t_{sol}} \left[\frac{dT}{dt} - \left(\frac{dT}{dt}\right)_c\right] \quad (3)$$

where: c_p – heat capacity, t_n - time recorded where nucleation temperature occurs, t_s – time recorded when solidus temperature was reached, m – mass (kg).

2.4 Microstructure examinations

Metallographic samples were taken from a location close to the thermocouple tip. Samples were cold mounted and grounded on 240, 320, 400, 600 and 1200 grit SiC paper and then polished with 6 μm, 3 μm and 1 μm diamond paste. In order to reveal the structure, polished section was etched using the Keller's etchant (0.5 ml HF, 1.5 ml HCl, 2.5 ml HNO_3, 95.5 ml H_2O) immersed for 15 s as recommended time. Microstructure features were characterized using light optical microscope Leica Q - WinTM image analyser.

The X-ray qualitative and quantitative microanalysis and the analysis of a surface distribution of cast elements and shape, in the examined aluminium cast alloy have been made on the scanning electron microscope ZEISS SUPRA 35 with a system EDAX XM4 TRIDENT consisting of: spectrometer EDS, WDS and EBSD. X-ray examinations of investigated aluminium alloy were made using a X'Pert Pro diffractometer with Cu anode. Diffraction examinations were performed within the range of angles from 20º to 90º. The measurement step was 0.05º in length whilst the pulse counting time was 5 s.

3. Investigation results

Representative heating and cooling curve of the ENAC-51500 alloy solidify without interruption by a quench is presented on (Fig. 1) with pointed typical metallurgical reaction for this alloy. It can be noted that for heating and non-equilibrium cooling significant differences between heating and cooling metallurgical reactions are present i.e. $\Delta T = T_{melting} - T_{solidus} \approx 22\ °C$. The temperature shift between heating and cooling events (the so called metallurgical hysteresis) is caused by the non-equilibrium solidification process. This information is of paramount importance since many published papers wrongly use the solidification thermal analysis data for optimization of the heat treatment parameters.

Definitions and measured values of the characteristic points associated with individual non-equilibrium metallurgical events taking place during both melting and solidification processes pointed on (Fig. 1) presents in Table 2 and 3.

Based on (Fig. 1) the thermal (metallurgical events) are not clear visible, therefore the first derivative is needed precise determination of curve characteristics (Fig. 2). As can be observed, the alloy does not start to solidify immediately at the equilibrium solidification temperature because no effective nuclei are present. Some undercooling is needed to supply the driving force for the nucleation and growth of the aluminium dendrites. Latent heat evolves and causes the temperature of the surrounding melt to rise. With further melt cooling, the dendrites continue to grow.

Based on the first derivative (Fig. 2), the α-Al Dendrite Nucleation Temperature, ($T^{\alpha DEN}{}_{NUC}$) (point 1) which represents the point at the primary stable dendrites start to solidify from the melt was found at 616.14 °C. This event is manifested by the change in the slope of the cooling curve and determined by the first derivative inflection point. The liquidus temperature signifies the beginning of the fraction solid that, at this point, is equal to zero.

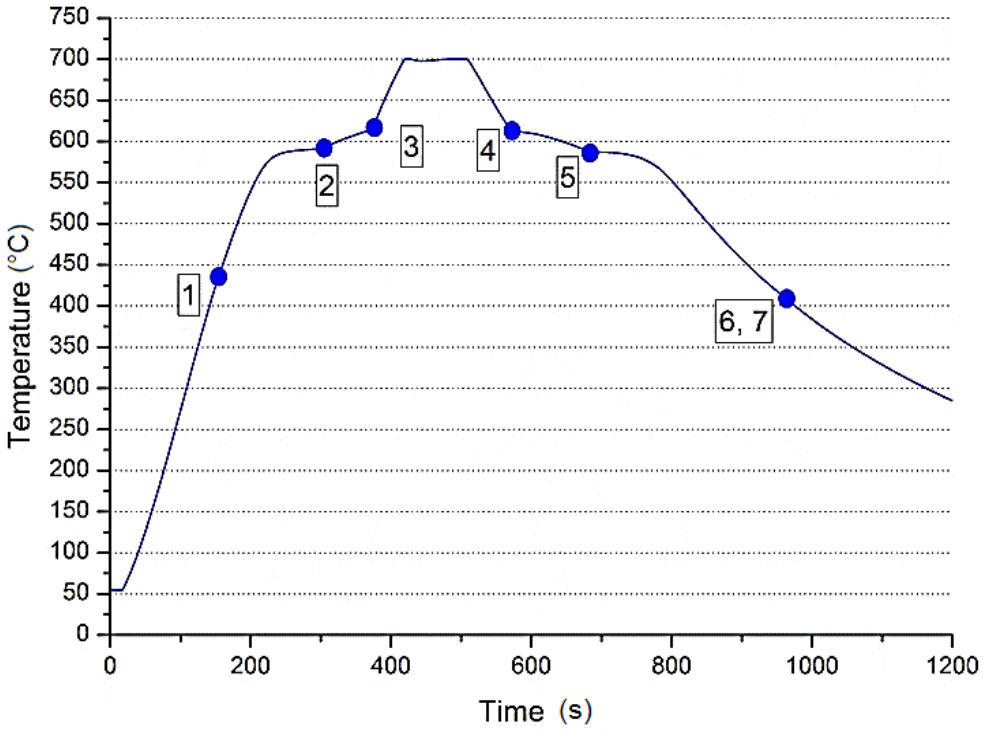

Fig.1. Representative Heating and Cooling curve of the ENAC-51500 alloy.

Table 2

Heating cycle thermal characteristics for analysed aluminium alloy.

Points	Thermal Characteristics	Heating Rate (0.8 ºC/s)
		Temperature (°C)
1	Start (beginning) of the alloy melting process	436.50
2	Melting of the Al-Mg-Si eutectic	592.02
3	Finish (end) of the alloy melting process	619.69
	Melting range	183.20

Table 3

Cooling cycle thermal characteristics for analysed aluminium alloy.

Points	Thermal Characteristics	Cooling Rate (0.5 ºC/s)
		Temperature (°C)
4	Nucleation of the Al dendrite network (liquidus temperature)	616.14
5	Nucleation of the Al-Mg-Si eutectic	589.08
6	Nucleation of the Mg enriched and other phases	434.48
7	Finish (end) of the alloy solidification process (Solidus Temperature)	414.08
	Solidification range	202.06

The next characteristic point on the crystallization curve was observed at 611.52° C. This is the α-Al Dendrite Minimum (Undercooling) Temperature, ($T^{\alpha DEN}{}_{MIN}$) (point 2) which represents a state where the nucleated dendrites have grown to such an extent that the liberated latent heat of fusion balances the heat extracted from the test sample. The $T^{\alpha DEN}{}_{MIN}$ as the local minimum is determined by the point at which the first derivative intersects the zero line ($dT/dt = 0$). Point 3 is the point in which produced α dendrites in liquid melt become coherent ($T^{\alpha DEN}{}_{DCP}$). In this point, the second derivative of the cooling curve intersects the zero line. The $T^{\alpha DEN}{}_{DCP}$ was noted at temperature 611.72 °C. After passing this point, the melt temperature increases

to a steady state growth temperature ($T^{\alpha DEN}{}_G$) (point 4). The $T^{\alpha DEN}{}_G$ corresponds to the second zero point on the first derivative curve ($dT/dt = 0$) following the start of nucleation ($dT/dt = 0$). This event was observed at 611.98 °C.

During crystallization process next characteristic point was observed at 611.24 °C which relates to next metallurgical reaction which comes from precipitation of $Al_{15}(FeMn)_3Si_2$ (point 5). Follow the first derivative curve it can be observed that the solidification rate (dT/dt, °C/sec) begins to slow down to almost zero, which is a results of larger latent heat of the eutectic phases formed by Mg_2Si and α-aluminium. As a result of continuous cooling of the aluminium alloy, Al+Mg_2Si Eutectic Nucleation Temperature ($T^{AlSi}{}_{E,NUC}$) occurs at 589.08 °C (point 6). This event is signified by a change in the slope of the cooling curve and is manifested by the first derivative (dT/dt) inflection point. The $T^{AlSi}{}_{E,NUC}$ represents the Al+Mg_2Si eutectic nucleation temperature at which a stablenucleation of co-precipitating first Mg and Si crystals and Al from the interdendritic melt begin to form cells that start to grow.

At 586.73 °C occurs the Al+Mg_2Si Eutectic Minimum Temperature, ($T^{AlSi}{}_{E,MIN}$) (point 7) which is characterized as a next local minimum on the cooling curve and is defined as the point at which the first derivative intersects the zero line following the Al-Si nucleation temperature ($dT/dt = 0$).

Next characteristic temperature at 587.13 °C (point 8) during crystallization process noted on first derivative curve is Al+Mg_2Si Eutectic Growth Temperature, ($T^{AlSi}{}_{E,G}$). This point corresponds to the second zero point on the first derivative curve following the Al-Si eutectic nucleation temperature ($dT/dt = 0$).

Nucleation of the Al_3Mg_2 enriched phases (point 9) were observed at 434.48 °C and solidus temperature T_{sol} (point 10) where crystallization process is finished was at 414.08 °C.

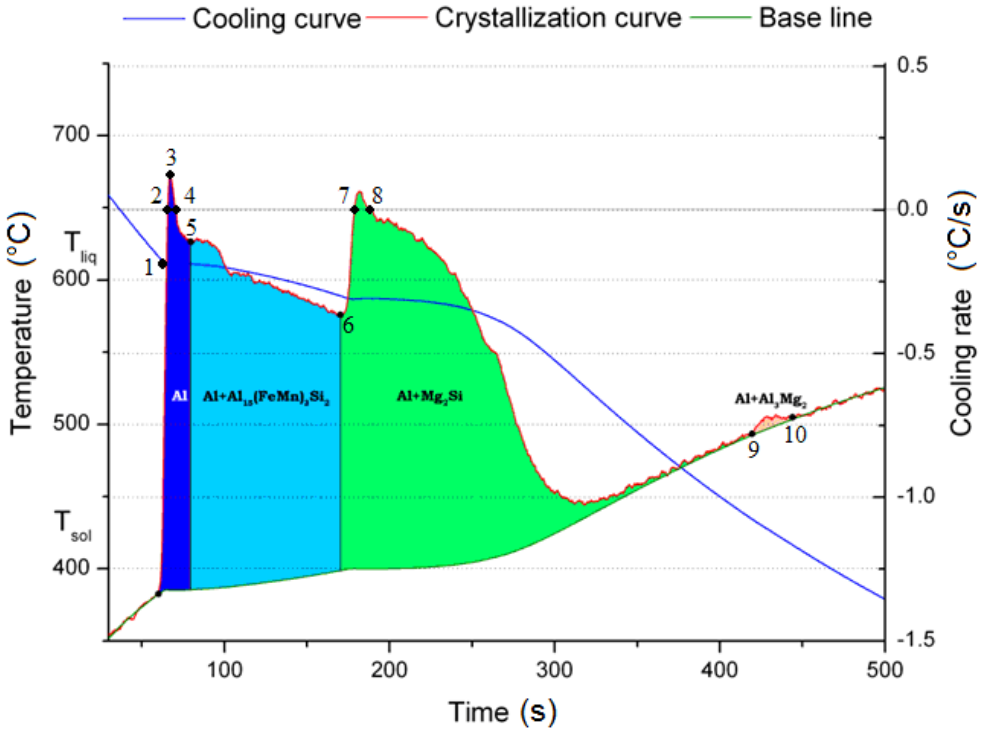

Fig. 2. Representative cooling, crystallization and base curves with characteristics points of crystallization process of ENAC-51500 aluminium alloy solidify at 0.5 °C/s.
(full colour version available online)

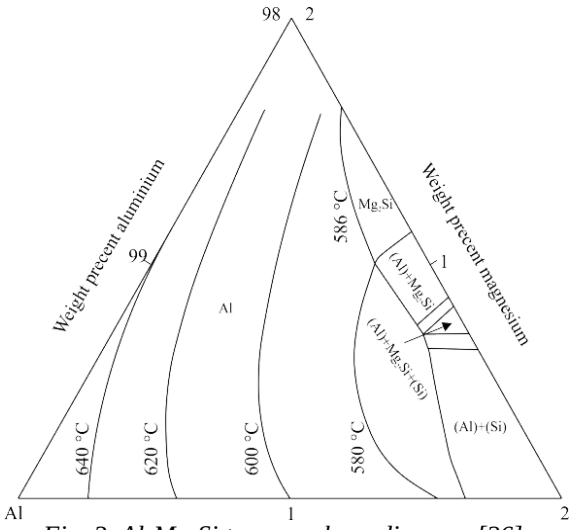

Fig. 3. Al-Mg-Si ternary phase diagram [26].

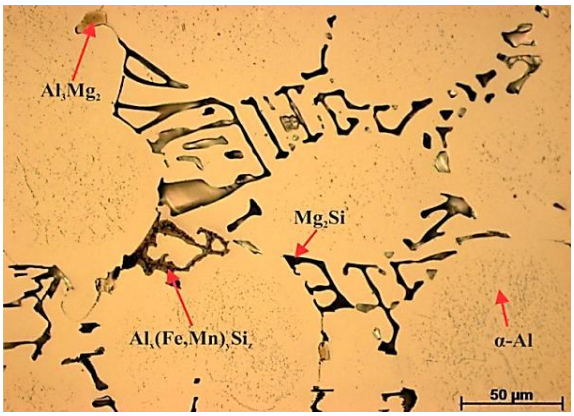

Fig. 4. Microstructures of ENAC-51500 alloy solidified with 0.5° C/s cooling rate. (full colour version available online)

Table 4

Latent heat of crystallization emitted during solidification and its participation in general latent heat of ENAC-51500 during solidification at cooling rate of 0.5 °C/s (From equation 3).

Specific heat in liquid state C_{pl} (J/g·°C)	**Specific heat in solid state C_{ps} (J/g·°C)**		**Weight (g)**
1.08	0.9		13.29
Reactions during solidification (temp. °C)	Latent heat of crystallization process		Participation (%)
	Per sample (J)	Per 1 gram of sample (J/g)	
L→Al, dendritic network (611.52°C)	302.9	22.8	9.7
L→Al+Al_{15}(Fe, Mn)$_3Si_2$ (611.24°C)	1287.3	96.9	42
L→Al+Mg_2Si (589.08°C)	1482.1	111.5	48.1
L→Al+Al_3Mg_2 (434.48°C)	7.8	0.6	0.2
Total	3080.1	231.8	100.0

On the (Fig. 2) there is also presented the thermal analysis data of aluminium alloyduring solidification at a cooling rate of 0.5 °C/s (Eq. 1) with marked areas of the individual components crystallizing during solidification process.

The solidification sequence is influenced to a considerable extent by the presence of iron and manganese, which elements together with aluminium and silicon start to precipitate just after formation of the dendritic network. Solidification starts with the formation of a dendritic network of aluminium and this is immediately followed by precipitation of $Al_{15}(FeMn)_3Si_2$.

Precipitation of $Al_{15}(FeMn)_3Si_2$ phase continuing down to the quasi-ternary eutectic reaction, where it continues to precipitate, the Mg_2Si phase. Based on binary alloy system Al-Mg the last final reaction with small thermal effect belongs to precipitation of the Al_3Mg_2 phase.

Table 4. contains precipitation sequence and the latent heat of crystallization. In accordance with the Al-Mg-Si phase diagram (Fig. 3) [26], investigated alloy should contain (α-Al + Mg_2Si) phases. However the analysis of Al-Mg binary diagram allows conclusion that there is also possibility of forming β-Al_3Mg_2 phase where morphology of this precipitation is relevant for the mechanical properties of the alloy. The selected typical structures of ENAC-51500 alloy, carried on light microscope are shown on (Fig. 4). Analysis of the microstructure indicates, that examined material consist α-Al

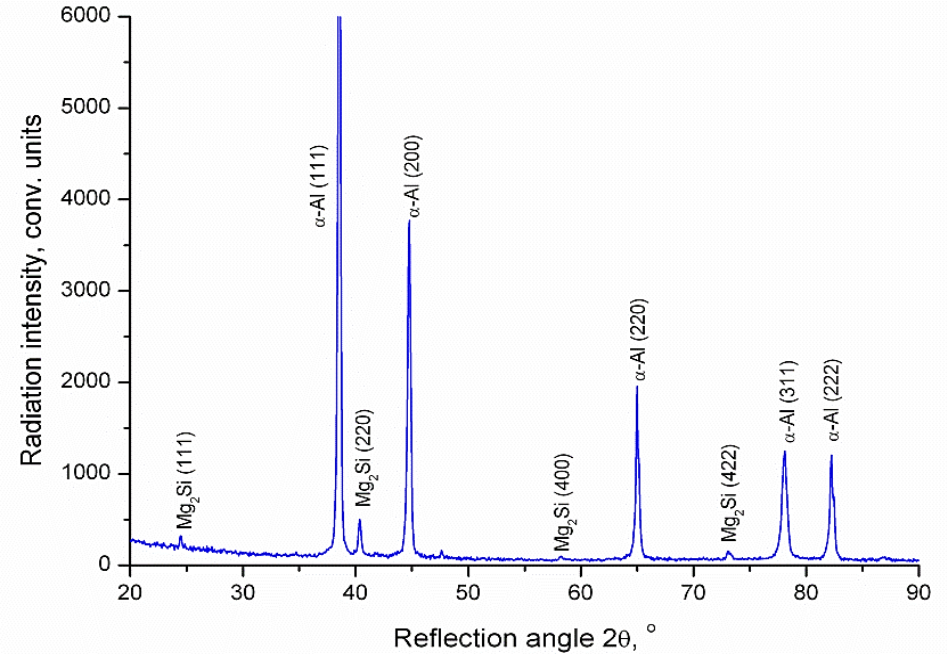

Fig. 5. XRD pattern of aluminium alloy.
(full colour version available online)

solid solution matrix (bright field) with Mg_2Si (dark precipitations) and β-Al_3Mg_2 (light precipitations) which are located on grain boundaries. There are also visible slight precipitations with irregular shape localized near the Mg_2Si phase, which probably is cubic $Al_{15}(FeMn)_3Si_2$. In Al-Si unmodified and slowly solidified cast components made from hypoeutectic alloys, the eutectic silicon (Si) crystals grow in a faceted manner in the form of large brittle flakes that are observable on (Fig. 4).

Since it's difficult to make a precise identification of intermetallics using only one method (e.g. microscopic examination) therefore XRD method was used to ensure confidence in the results of phase identification based on metallographic study. Using X-ray phase analysis it was found the presence of Mg_2Si phase and α-Al which is an alloy matrix as confirmed by metallographic study which is shown on the diffraction pattern (Fig. 5). X-ray phase analysis did not confirm the presence of β-Al_3Mg_2 and phases containing Fe and Mn, which may indicate that, mass concentration of these precipitations is below the detection limit of this method and suggested that the volume fraction of these phases is below 3 %.

An EDS quantitative (Table 5) and (Fig. 7a - 7d) analysis confirmed the presence of main alloying elements in the investigated alloy. SEM micrographs combined with X-ray spot microanalysis for the ENAC-51500 cast after thermal analysis, performed to identify morphology of the observed phases are shown in (Fig. 6). Structure observation prepared on scanning electron microscope and quantitative analysis confirmed the presence of eutectic phase α+β, and Mg_2Si intermetallic forming a characteristic particle shape called "Chinese script". Mg_2Si phase has an important influence on properties. It's solid solubility in the aluminium matrix is temperature dependent and causes hardening effects, which are utilized in technical alloys. In addition using an EDS analysis it was found occur of phases containing Mn and Fe, which stoichiometric composition is similar to $Al_{15}(FeMn)_3Si_2$ phase. The stoichiometry of Fe-bearing particles depends on the Si and Mn amounts. Iron usually combines with Si and Al to form Al_8Fe_2Si or $Al_{12}FeSi$ in low magnesium content alloys, or Al_3Fe in the absence of Mg. In case of increased amount of Mn, other particles may be present, such as: $Al_{15}(Fe,Mn)_3Si_2$ and $Al_6(Fe,Mn)$. Because the size of particular

elements of the structure is, in a prevailing measure, smaller than the diameter of the analysing beam, the obtained at the quantitative analysis chemical composition may be averaged as a result of which some values of element concentrations may be overestimated.

Microhardness (Table 6) test showed that, individual precipitations, formed during solidification process, are characterized by different hardness. It was observed that the lowest hardness about 65 HV exhibits α-Al solid solution and Mg_2Si phase. However structure investigation carried out earlier, indicates that, this alloy contain also Al_3Mg_2 and Fe-rich phases. It is expected that precipitations, which contain Fe should be characterized by higher hardness. Microhardness measurement revealed the presence of high hardness phases which causes a strengthening effect in this alloy.

An average value of microhardness was about 172 HV which confirms that in $AlMg_5Si_2Mn$ alloy are present hard $Al_{15}(FeMn)_3Si_2$ phases. In addition it was observed the presence of small bright precipitations Al_3Mg_2 which microhardness was about 117 HV. Hardness measurement which was carried out using Rockwell method, showed that an alloy after remelting process is characterized by lower hardness (74.46 HRF after remelting, 81.15 HRF as cast state), which could be caused by microporosity formed during solidification process.

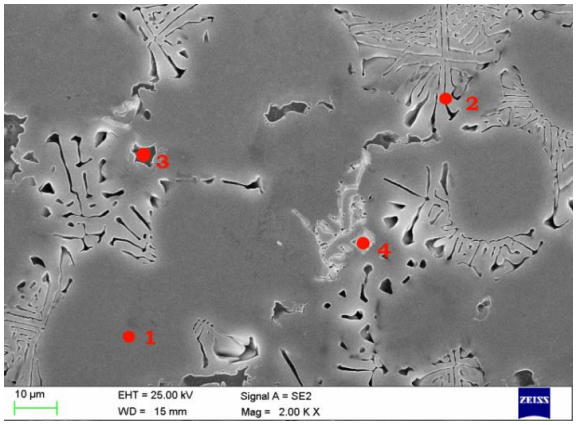

Fig. 6. Representative scanning electron microscope micrograph of aluminium alloy solidify at 0.5 °C/s. (full colour version available online)

Table 5

Pointwise chemical composition analysis from Fig. 6.

Point	Element	The mass concentration of main elements (%)	
		weight (%)	atomic (%)
1	Mg	3.56	3.93
	Al	96.44	96.07
2	Mg	5.44	6.02
	Al	86.66	86.41
	Si	7.90	7.57
3	Mg	29.65	31.87
	Al	70.35	68.13
4	Mg	2.33	2.89
	Al	68.43	76.5
	Si	1.97	2.12
	Mn	12.30	6.75
	Fe	11.48	6.20

Table 6

Microhardness of the examined aluminium alloy after thermal analysis.

Phase	Average microhardness $HV_{0,05}$
α-Al	64.22
Al_3Mg_2	117.50
Mg_2Si	65.35
$Al_{15}(FeMn)_3Si_2$	172.21

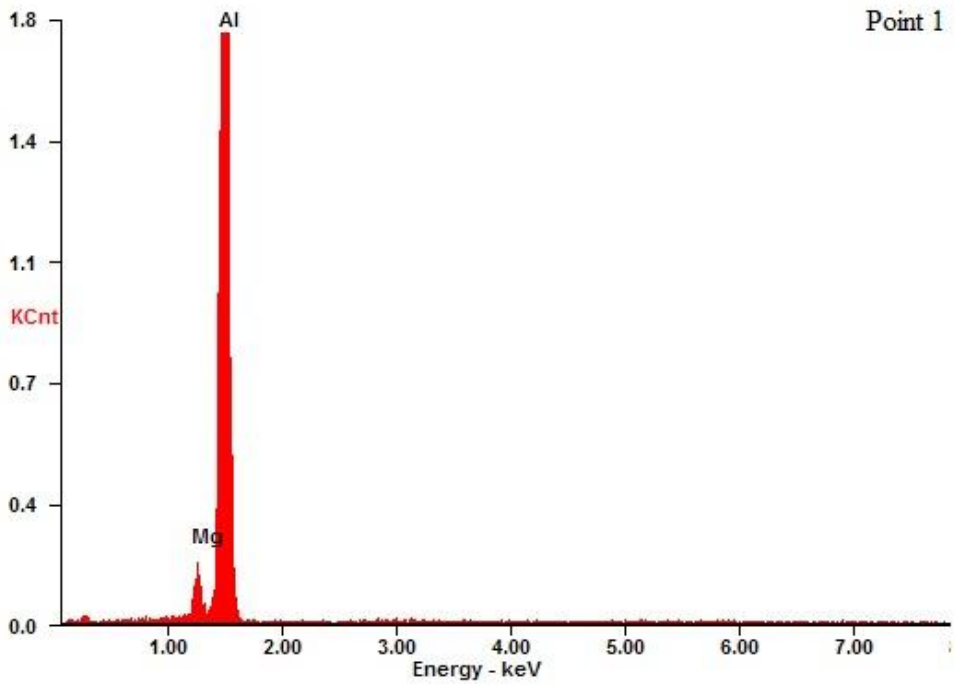

a)

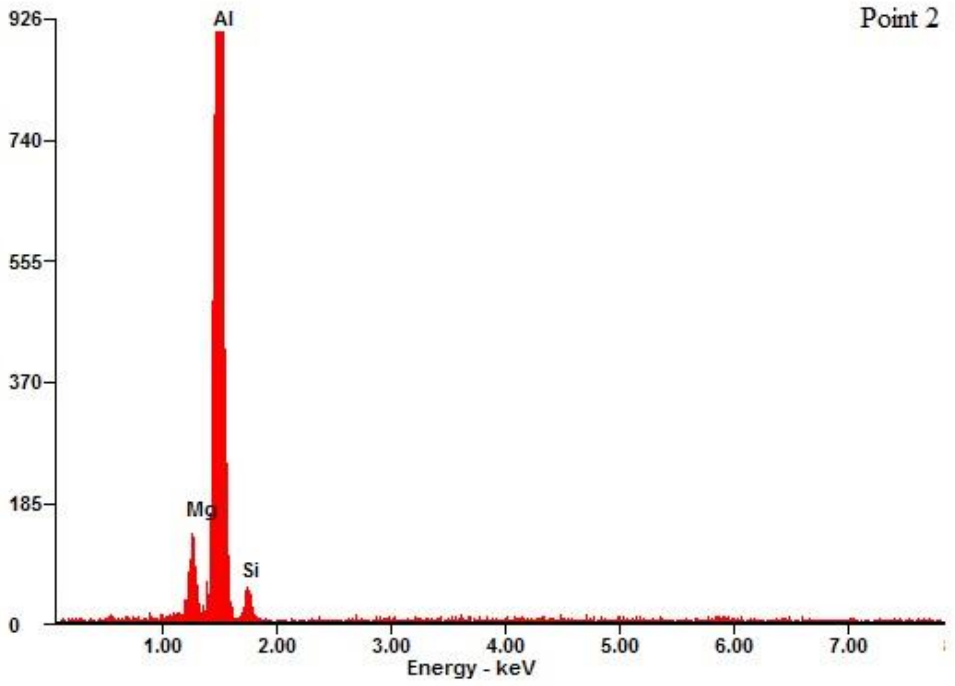

b)

Fig. 7. The EDS spectrums from a) Point 1, b) Point 2, c) Point 3, d) Point 4.
(full colour version available online)

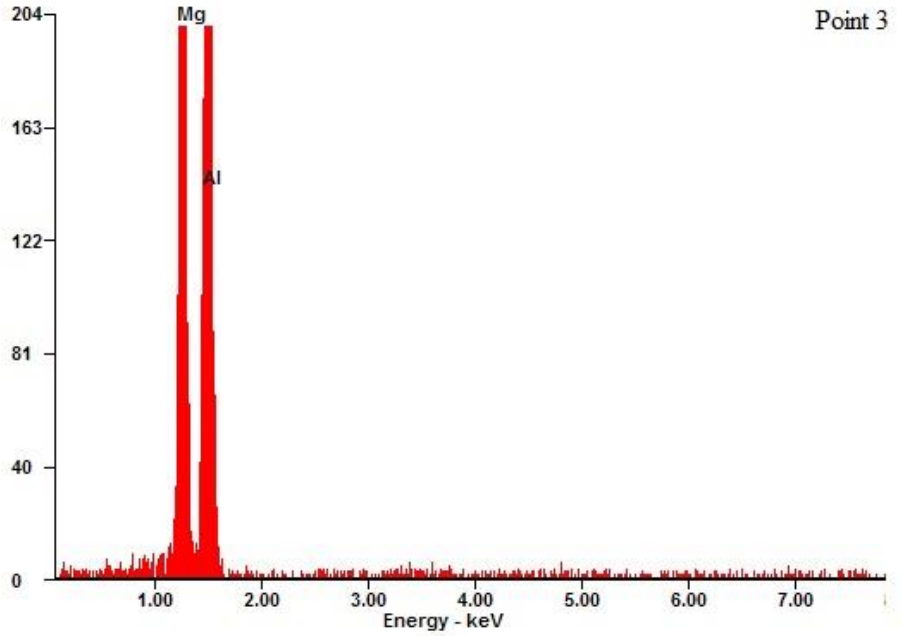

c)

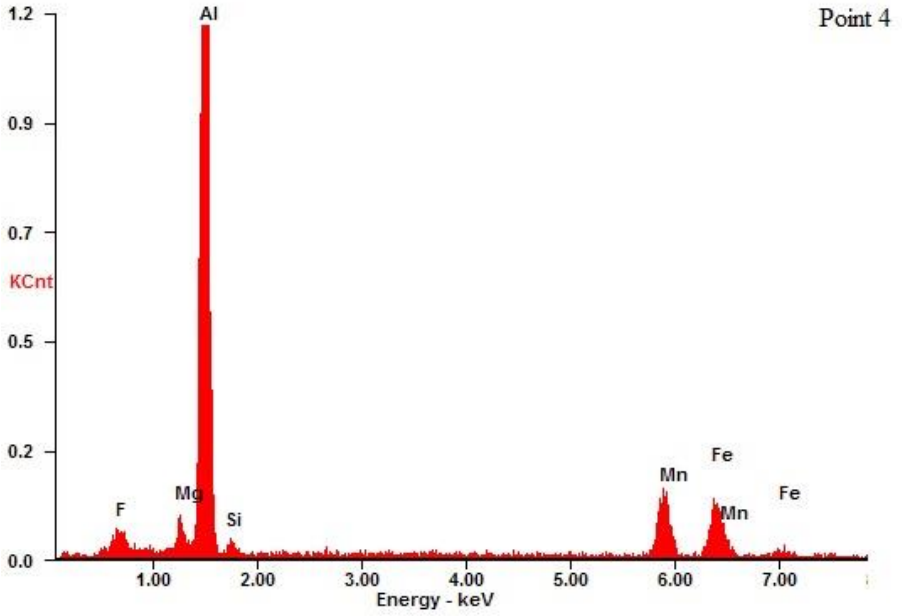

d)

Continuing of Fig. 7. The EDS spectrums from a) Point 1, b) Point 2, c) Point 3, d) Point 4.
(full colour version available online)

Summary

Critical sections of the cast component(s) containing large flakes of Si have poor mechanical properties and poor machinability characteristics. Therefore the commercial application of these alloys often depends on chemical, thermal (rapid solidification and heat treatment) modification of the eutectic Si crystals. Knowledge about crystallization process significantly simplifies the design process of heat treatment in order to modify the aluminium alloys. It is interesting to note that the thermal analysis of the heating cycle allows for the development of an optimum two and/or multiple-step solution treatment capable of improving the dissolution of the soluble phases (including the Cu rich ones) and which results in achieving significantly higher mechanical characteristics in the thick (slowly solidified) section of the automotive components. It is well known that the nucleation ($T^{AlSi}_{E,NUC}$) and growth

($T^{AlSi}_{E,G}$) temperatures of the eutectic Si are depressed by the addition of modifiers. As the results show that this value is above the eutectic temperature can be concluded that the used aluminium alloy in experiment is unmodified which also confirmed by the microstructure examinations. In experiment eutectic solidification occurs at a temperature up to 10 °C above the equilibrium eutectic temperature.

The results and parameters obtained from thermal analysis can be applied in metal casting industry for selecting aluminium ingot preheating temperature for semi solid processing.

Acknowledgement

This paper has been partially elaborated in the framework of the project „Support research and development in the Moravian-Silesian Region 2013 DT 1 - International research teams" (02613/2013/RRC) - financed from the budget of the Moravian-Silesian Region Czech Republic on the base of co-operation with VŠB – Technical University of Ostrava, Faculty of Mechanical Engineering.

References

[1] Ł. Kaczmarek, P. Kula, J. Sawicki, S. Armand, T. Castro, P. Kruszyński, A. Rochel: Arch. Metall. Mater. 54 (4) (2009) 1199-1205.

[2] W. Moćko, Z. Kowalewski: Journal of KONES, 19 (2) (2012) 345-351.

[3] S. Das: JOM 52 (8) (2000) 41-44.

[4] http://www.economist.com/node/21558269.

[5] H. He, A. Bandivadekar: Passenger car fuel-efficiency, 2020-2025 Comparing stringency and technology feasibility of the Chinese and US standards, The International Council on Clean Transportation. 2013.

[6] J. Liu: Mater. Sci. Forum 519-521 (2006) 1233-1238.

[7] W. Miller: Mater Sci Eng 280 (1) (2008) 37-49.

[8] M. Krupinski, L.A. Dobrzanski, J.H. Sokolowski, W. Kasprzak, G. Byczynski: Mater. Sci. Forum 539-543 (1) (2007) 339-344.

[9] R. Holmestad, R. Bjorge, F. Ehlers, M. Torsaeter, C. Marioara, S. Andersen: J Phys. Conf. Ser. 371 (2012) 1-6.

[10] F. Farh, K. Djemmal, R. Guemini, F. Serradj: Ann. Chim. - Sci. Mat. 35 (5) (2010) 283-289.

[11] T. Tański, K. Labisz: Solid State Phenom. 186 (2012) 192-197.

[12] T. Tański: Stroj Vestn - J Mech E 59/3 (2013) 165-174.

[13] L.A. Dobrzański, T. Tański, J. Trzaska: Mater. Sci. Forum 638-642 (2010) 1488-1493.

[14] T. Tański, L.A. Dobrzański, L. Čížek: Adv. Mat. Res. 15-17 (2007) 491-496.

[15] L.A. Dobrzański, M. Krupiński, K. Labisz, B. Krupińska, A. Grajcar: Mater. Sci. Forum 638-642 (2010) 475-480.

[16] Y. Birol: Mater. Charact. 73 (2012) 37-42.

[17] H.B. Michael Rajan, S. Ramabalan, I. Dinaharan, S. Vijay: Arch. Civ. Mech. Eng. 14 (1) (2014) 72-79.

[18] M. Pietrzyk, Ł. Madej, Ł. Rauch, R. Gołąb: Arch. Civ. Mech. Eng. 10 (4) (2010) 57-67.

[19] L.A. Dobrzański, T. Tański, Sz. Malara, M. Król J. Domagała-Dubiel: In: Magnesium Alloys - Design, Processing and Properties, Ed: F. Czerwinski, InTech, Croatia, 2011 pp. 321-350.

[20] L.A. Dobrzański, T. Tański, S. Malara, M. Król: Mater. Sci. Forum 674 (2011) 11-18.

[21] H. Englehardt, B. Hallstedt, M. Drue, A. Loeffler, M. Schick, M. Rottenmayr: Adv. Eng. Mater. 14 (5) (2012) 319-323.

[22] L. Backerud, G. Chai, J. Tamminen: Solidification characteristics of aluminium alloys Vol. 2 Foundry Alloys, AFS SkanAluminium, Stockholm, Sweden 1990.

[23] L. Backerud, G. Chai: Solidification characteristics of aluminium alloys Vol. 3 Foundry Alloys, AFS SkanAluminium, Stockholm, Sweden 1992.

[24] L. Backerud, E. Król, J. Tamminen: Solidification characteristics of aluminium alloys Vol. 1 Wrought Alloys, AFS SkanAluminium, Oslo, Sweden 1986.

[25] Method and Apparatus for Universal Metallurgical Simulation and Analysis; United States Patent, Patent No.: US 7354491 B2, Apr. 8. 2008.

[26] T.B. Massalski, J.L. Murray, L.H. Bennet, and H. Baker, Binary Alloy Phase Diagrams, Vol 1 and 2, American Society for Metals, Metals Park, OH, 1986.